

# Dephasing-assisted Gain and Loss in Mesoscopic Quantum Systems

Clemens Müller and Thomas M. Stace

*ARC Centre of Excellence for Engineered Quantum Systems, School of Mathematics and Physics,  
University of Queensland, Saint Lucia, Queensland 4072, Australia*

(Dated: January 31, 2017)

Motivated by recent experiments, we analyse the phonon-assisted steady-state gain of a microwave field driving a double quantum-dot in a resonator. We apply the results of our companion paper, which derives the complete set of fourth-order Lindblad dissipators using Keldysh methods, to show that resonator gain and loss are substantially affected by dephasing-assisted dissipative processes in the quantum-dot system. These additional processes, which go beyond recently proposed polaronic theories, are in good quantitative agreement with experimental observations.

Microwave-driven double-quantum dots (DQD) have demonstrated a rich variety of quantum phenomena, including population inversion [1–5], gain [6–8], masing [9–14] and Sysiphus thermalization [15]. These processes are well understood in quantum optical systems, however mesoscopic electrostatically-defined quantum dots exhibits additional complexity not typically seen in their optical counterparts, arising from coupling to the phonon environment.

A notable experimental example of this, which motivates our work, is an electronically open, DQD system coupled to a driven resonator, pictured in Fig. 1a,b, [7]. Substantial gain in the resonator field was observed when the DQD is blue-detuned with respect to the resonator, and capacitively biased to induce substantial population inversion. The observed gain is attributed to correlated emission of a resonator photon and a phonon into the semiconductor medium in which the DQD system is defined. This process ensures conservation of energy, since the phonon carries the energy difference,  $\hbar(\omega_q - \omega_r)$ , between the energy of the qubit and the energy of the resonator phonon (we set  $\hbar = 1$  for the rest of the letter).

In some experimental regimes of [7], the observed gain is well described by a theory based on a canonical transformation to a polaron frame [16]. In this frame, conventional quantum optics techniques and approximations (Born-Markov, secular etc) are used to derive dissipative Lindblad superoperators that are quadratic in both the qubit-phonon bath coupling strength,  $\beta_j$ , and in the qubit-resonator coupling strength,  $g$ . However the same theory fails to describe substantial loss (sub-unity gain) in other experimental regimes, which strongly suggests that there are additional dissipative processes that are not captured in the polaron frame.

One problem with relying on a canonical transformation as the basis for a perturbative expansion is that it is tailored to a specific frame, which emphasises some processes over others. It is therefore not guaranteed to find all dissipative processes that occur at a given order in perturbation theory.

In a longer technical companion paper [17], we consider a generic two-level system (qubit) coupled to a resonator, and to a bosonic bath, and we present a derivation of the

complete set of Lindblad superoperators that arise at the same order as those in [16], i.e.  $\sim O(\beta_j^2 g^2)$ . Our derivation is based on Keldysh diagrammatic perturbation theory, and makes explicit the nature of the approximations and idealisations we deploy. In Ref. 17 we show that as well as the correlated decay processes in Ref. 16, we find a number of additional Lindblad dissipators at the same perturbative order. Amongst these additional dissipators, there is a process describing correlated dephasing of the qubit accompanied by resonator photon emission or absorption. This leads to additional qubit-mediated resonator gain and loss terms, which we believe have not been derived previously in the Lindblad formalism.

In this Letter, we apply the results of our companion paper [17] to the specific problem of the open DQD system coupled to a driven resonator and to a phonon environment. We show that the additional Lindblad dissipators that arise in the Keldysh analysis of the Dyson series do indeed generate substantial additional loss, and that the resulting theory consistently accounts for the magnitude of the gain and loss in different experimental regimes.

In what follows, the ‘system’ consists of the resonator and the DQD (pictured in Fig. 1a), which is driven at frequency  $\omega_d$  and amplitude  $\epsilon_d$ , and the ‘bath’ is the environment of phonon modes,  $b_j^\dagger$ . Interactions between the DQD and the resonator photons and bath phonons will be treated perturbatively. As such, we partition the total Hamiltonian as  $H = H_S + H_D + H_B + H_I$ , where

$$\begin{aligned} H_S &= \omega_r a^\dagger a - \epsilon_q \sigma_z^{(p)} / 2 + \Delta_q \sigma_x^{(p)} / 2, \\ H_D &= \epsilon_d (a^\dagger e^{i\omega_d t} + a e^{-i\omega_d t}) / 2, \\ H_B &= \sum_{\text{modes } j} \omega_j b_j^\dagger b_j, \\ H_I &= g \sigma_z^{(p)} (a + a^\dagger) / 2 + \sigma_z^{(p)} X / 2, \end{aligned}$$

where  $\sigma_z^{(p)} = |R\rangle\langle R| - |L\rangle\langle L|$  and  $\sigma_x^{(p)} = |R\rangle\langle L| + |L\rangle\langle R|$  are DQD operators expressed in the position basis  $\{|L\rangle, |R\rangle\}$  (shown in Fig. 1b),  $a$  is the resonator annihilation operator, and  $X = \sum_j \beta_j (b_j + b_j^\dagger)$  is the phonon coupling operator.

We transform to an interaction frame defined by  $H_0 = H_S + H_B$ , so that the interaction Hamiltonian in

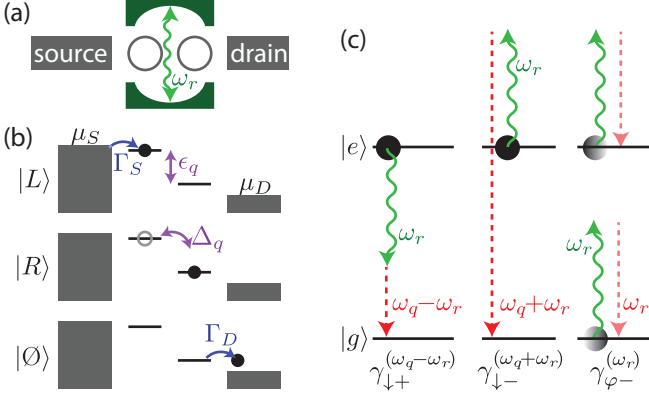


Figure 1. (a) Schematic showing a double quantum dot (DQD) coupled to a cavity resonator mode, and to source/drain leads. (b) An electron (black dot) tunnels from the source lead to the DQD state  $|L\rangle$ , which couples to the DQD state  $|R\rangle$  with matrix element  $\Delta_q$ , and then tunnels to the drain, leaving the DQD in the empty state  $|\emptyset\rangle$ . Also shown are inter-dot bias,  $\epsilon_q$ , and coupling rates  $\Gamma_{S,D}$  to metallic leads, with chemical potentials  $\mu_{S,D}$ . (c) Dissipative processes due to phonon emission (dashed arrows) responsible for rates in Eq. 5. Each process is correlated with resonator photon creation (downward wiggly arrows) or annihilation (upward wiggly arrows);  $\gamma_{\downarrow\pm}^{(\omega_q \pm \omega_r)}$  correspond to DQD relaxation from  $|e\rangle$  to  $|g\rangle$ , whilst  $\gamma_{\varphi-}^{(\omega_r)}$  corresponds to DQD dephasing, leaving the populations of  $|e\rangle$  and  $|g\rangle$  unchanged.

the DQD energy eigenbasis becomes

$$H_I(t) = g (\cos \theta \sigma_z + \sin \theta \sigma_x(t)) (ae^{-i\omega_r t} + a^\dagger e^{i\omega_r t}) / 2 + (\cos \theta \sigma_z + \sin \theta \sigma_x(t)) X(t) / 2, \quad (1)$$

where  $\sigma_z = |g\rangle\langle g| - |e\rangle\langle e|$ ,  $\sigma_x(t) = e^{i\omega_q t} |e\rangle\langle g| + \text{h.c.}$ ,  $\tan \theta = \Delta_q / \epsilon_q$ ,  $\omega_q = (\epsilon_q^2 + \Delta_q^2)^{-1/2}$  is the DQD energy splitting, and  $X(t) = \sum_j \beta_j (b_j e^{-i\omega_j t} + b_j^\dagger e^{i\omega_j t})$ .

We have made a rotating wave approximation in  $H_D$ , and we also assume weak coupling between the system and bath. Further, in the experiment we consider,  $g \ll |\omega_q - \omega_r|$ . Within these approximations we derive a Lindblad master equation in the interaction Hamiltonian  $H_I(t)$ , using Keldysh perturbative methods. Different dissipative processes arise at different orders of the DQD-resonator and DQD-phonon coupling strengths.

The dynamics of the open DQD-resonator system are governed by the master equation

$$\dot{\rho} = -i[H_D(t), \rho] + \mathcal{L}_2 \rho + \mathcal{L}_4 \rho + \mathcal{L}_{\text{leads}} \rho. \quad (2)$$

In this expression, the resonator driving hamiltonian coherently populates the resonator, and the DQD-phonon and DQD-resonator coupling gives rise to dynamical superoperators  $\mathcal{L}_2$  and  $\mathcal{L}_4$  at different orders of perturbation theory in the coupling strengths  $g$  and  $\beta_j$ . Electronic coupling to the leads gives rise to the dissipators  $\mathcal{L}_{\text{leads}}$ . In what follows, we explain these different contributions

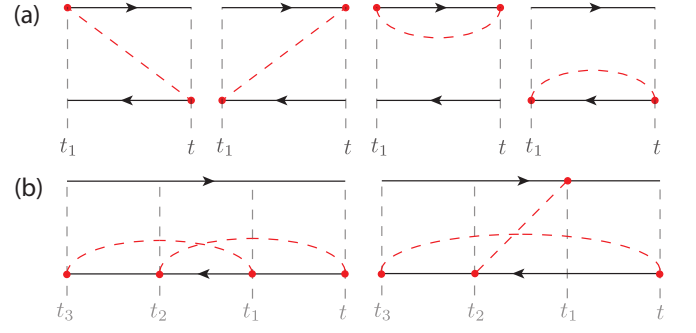


Figure 2. (Color online) (a) Diagrams representing all 2nd order terms in the Keldysh self-energy. (b) Two examples of irreducible fourth-order Keldysh diagrams. All 32 irreducible diagrams at this order can be generated from the two shown by swapping sub-sets of interaction vertices between the lower and upper lines. For more details, see Ref. 17.

in more detail, and then evaluate the steady state gain and loss implied by Eq. 2.

The second-order dispersive and dissipative terms generated by phonon and cavity coupling are [18, 19]

$$\mathcal{L}_2 \rho = -i[H_2, \rho] + \gamma_{\downarrow,2} \mathcal{D}[\sigma_-] \rho + \gamma_{\uparrow,2} \mathcal{D}[\sigma_+] \rho + \gamma_{\varphi,2} \mathcal{D}[\sigma_z] \rho + \kappa_{-,r} \mathcal{D}[a] \rho + \kappa_{+,r} \mathcal{D}[a^\dagger] \rho, \quad (3)$$

where  $\gamma_{\downarrow,2} = \sin^2 \theta C(\omega_q)/2$ ,  $\gamma_{\uparrow,2} = \sin^2 \theta C(-\omega_q)/2$  and  $\gamma_{\varphi,2} = \cos^2 \theta C(0)/2$  depend on the bath spectral function,  $C(\omega)$ , which is the Fourier transform of the bath correlation function,  $\langle X(t)X(0) \rangle$  [17, 19], arising from coupling to the bosonic environment,  $H_2 = \bar{\chi} \sigma_z (1 + 2a^\dagger a)$ ,  $\bar{\chi} = g^2 \sin^2 \theta \omega_q / (4\omega_q^2 - 4\omega_r^2)$  is the dispersive shift between the DQD and resonator, and  $\kappa_{-,r} = \kappa(n_{\text{th}} + 1)$  and  $\kappa_{+,r} = \kappa n_{\text{th}}$  depend on the cavity decay rate  $\kappa$  and the thermal population  $n_{\text{th}} = 1/(e^{\beta\omega_r} - 1)$ , with  $\beta = 1/k_B T$ . Lindblad superoperators are defined as  $\mathcal{D}[\mathcal{O}] \rho = \mathcal{O} \rho \mathcal{O}^\dagger - \{\mathcal{O}^\dagger \mathcal{O}, \rho\}/2$ . The first line of Eq. 3, which includes the dispersive DQD-resonator shift and phonon-induced relaxation, excitation and dephasing, can be obtained by standard quantum optical methods [2, 20], or equivalently, by evaluating the second-order Keldysh diagrams for the DQD-resonator and DQD-phonon interaction, shown in Fig. 2a.

The dissipators that arise at higher order are not part of the standard ‘canon’ of Lindblad superoperators in the quantum optical master equation. At a given perturbative order, the complete set can be found by evaluating the irreducible Keldysh self-energy diagrams at that order. The third-order contributions vanish. There are 32 irreducible diagrams at fourth order, two examples of which are shown in Fig. 2b. In practise, each vertex in a diagram needs to be decomposed into the 9 different Fourier components represented in Eq. 1, so that at 4<sup>th</sup> order, there are up to  $32 \times 9^4$  different diagrams to integrate.

These integrals can be evaluated analytically, and grouped into Lindblad dissipators with associated rates. This calculation is described in detail in [17], and results in a total of 21 individual Lindblad terms. As with  $\mathcal{L}_2$ , the rates depend on the bath spectral function,  $C(\omega)$ , and its derivatives [17, 21], evaluated at system frequencies  $\omega = 0, \pm\omega_q, \pm\omega_r, \pm(\omega_q \pm \omega_r)$  [2].

For the purposes of this Letter, we find six of the 21 Lindblad dissipators represent the dominant contribution to the correlated DQD-resonator decay, and thus to gain and loss in the resonator field. These are

$$\mathcal{L}_4 \bar{\rho} = \gamma_{\downarrow+}^{(\omega_q - \omega_r)} \mathcal{D}[\sigma_- a^\dagger] \rho + \gamma_{\downarrow-}^{(\omega_q + \omega_r)} \mathcal{D}[\sigma_- a] \rho \quad (4a)$$

$$+ \gamma_{\uparrow+}^{(-\omega_q - \omega_r)} \mathcal{D}[\sigma_+ a^\dagger] \rho + \gamma_{\uparrow-}^{(-\omega_q + \omega_r)} \mathcal{D}[\sigma_+ a] \rho \quad (4b)$$

$$+ \gamma_{\varphi+}^{(-\omega_r)} \mathcal{D}[\sigma_z a^\dagger] \rho + \gamma_{\varphi-}^{(\omega_r)} \mathcal{D}[\sigma_z a] \rho, \quad (4c)$$

where the rates are given by

$$\begin{aligned} \gamma_{\downarrow+}^{(\omega_q - \omega_r)} &= g^2 \cos^2 \theta \frac{\omega_q^2 \sin^2 \theta}{2\omega_r^2 (\omega_q - \omega_r)^2} C(\omega_q - \omega_r), \\ \gamma_{\downarrow-}^{(\omega_q + \omega_r)} &= g^2 \cos^2 \theta \frac{\omega_q^2 \sin^2 \theta}{2\omega_r^2 (\omega_q + \omega_r)^2} C(\omega_q + \omega_r), \\ \gamma_{\varphi-}^{(\omega_r)} &= g^2 \sin^2 \theta \frac{\omega_q^2 \sin^2 \theta}{2(\omega_q^2 - \omega_r^2)^2} C(\omega_r), \end{aligned} \quad (5)$$

$\gamma_{\uparrow-}^{(-\omega_q + \omega_r)} = \gamma_{\downarrow+}^{(\omega_q - \omega_r)} e^{-\beta(\omega_q - \omega_r)}$ ,  $\gamma_{\uparrow+}^{(-\omega_q - \omega_r)} = \gamma_{\downarrow-}^{(\omega_q + \omega_r)} e^{-\beta(\omega_q + \omega_r)}$  and  $\gamma_{\varphi+}^{(-\omega_r)} = \gamma_{\varphi-}^{(\omega_r)} e^{-\beta\omega_r}$ . The label  $\uparrow$  ( $\downarrow$ ) denotes a process that excites (relaxes) the DQD,  $\varphi$  denotes DQD dephasing, and  $+$  ( $-$ ) denotes photon creation (annihilation).

The terms in Eq. 4a,b have been derived elsewhere, based on a canonical transformation to a polaronic frame in which the qubit and the resonator are correlated [16]. They correspond to processes in which the qubit and the resonator both change state, accompanied by exchange of energy with the phonon bath. This is illustrated in the first two panels of Fig. 1c. The final two terms in Eq. 4c are processes that we believe have not been considered in the Lindblad formalism, and correspond to a DQD-mediated exchange of energy between the resonator and the phonon bath that leaves DQD populations unaffected, illustrated in the last panel of Fig. 1c.

In the experiments that motivate this Letter, the external leads couple to the open DQD, inducing a charge-discharge transport cycle, pictured in Fig. 1b. We extend the DQD basis to include the empty state  $|\emptyset\rangle$ , in which the DQD is uncharged. As electrons tunnel between the leads and the DQD, it passes transiently through the empty state. This process is described by the incoherent Lindblad superoperator [2, 20, 22]

$$\mathcal{L}_{\text{leads}} \rho = \Gamma_L \mathcal{D}[|L\rangle\langle\emptyset|] \rho + \Gamma_R \mathcal{D}[|\emptyset\rangle\langle R|] \rho. \quad (6)$$

For simplicity, we will assume  $\Gamma_R = \Gamma_L = \Gamma$ . Depending on the sign of  $\epsilon_q$ , the DQD population may become inverted in steady state.

Having established Eq. 2 describing the dynamics of the correlated DQD-resonator system we could in principle find the full, correlated steady-state of the system (in a suitably truncated basis). However, we anticipate that the resonator will be close to a coherent state  $|\alpha\rangle$ , so we proceed by making a mean-field approximation in each of the DQD and resonator subsystems. This also has the advantage of being computationally straightforward.

Thus, we factorise the system density matrix as  $\rho \approx \rho_r \otimes \rho_q$ , resulting in master equations for each subsystem, mutually coupled through the mean values  $\alpha$  and  $\langle\sigma_z\rangle$ . To proceed, we perform a displacement transformation on the resonator,  $a \rightarrow \tilde{a} + \alpha$  [23, 24] and also transform into a rotating frame defined by  $\omega_d \tilde{a}^\dagger \tilde{a}$ . In the displaced resonator frame, and after tracing over the DQD degrees of freedom, Eq. 2 reduces to a dynamical equation for the resonator

$$\dot{\rho}_r = -i[\tilde{H}_r, \rho_r] + \kappa_- \mathcal{D}[\tilde{a}] \rho_r + \kappa_+ \mathcal{D}[\tilde{a}^\dagger] \rho_r, \quad (7)$$

where

$$\begin{aligned} \tilde{H}_r &= (\delta\omega_r - 2\bar{\chi} \langle\sigma_z\rangle) \tilde{a}^\dagger \tilde{a} \\ &+ \tilde{a}^\dagger (\epsilon_d/2 + \alpha(\delta\omega_r + 2\bar{\chi} \langle\sigma_z\rangle - i\kappa'/2)) + \text{h.c.}, \end{aligned} \quad (8)$$

in which  $\delta\omega_r = \omega_r - \omega_d$ ,  $P_i = \text{Tr}_q \{\rho |i\rangle\langle i|\}$ ,  $\langle\sigma_z\rangle = P_g - P_e$ , and  $\kappa' = \kappa'_- - \kappa'_+$  is the DQD-renormalised resonator linewidth, which depends on

$$\begin{aligned} \kappa'_- &= \kappa_{-,r} + \gamma_{\downarrow-}^{(\omega_q + \omega_r)} P_e + \gamma_{\uparrow-}^{(-\omega_q + \omega_r)} P_g + \gamma_{\varphi-}^{(\omega_r)} (1 - P_\emptyset), \\ \kappa'_+ &= \kappa_{+,r} + \gamma_{\downarrow+}^{(\omega_q - \omega_r)} P_e + \gamma_{\uparrow+}^{(-\omega_q - \omega_r)} P_g + \gamma_{\varphi+}^{(-\omega_r)} (1 - P_\emptyset). \end{aligned} \quad (9)$$

For the parameter regime we consider below,  $P_\emptyset \ll 1$ .

The coefficient of  $\tilde{a}^\dagger$  in Eq. 8 describes effective driving of the displaced resonator mode  $\tilde{a}$ . We self-consistently choose the displaced frame to eliminate the effective driving, so that

$$\alpha = -\epsilon_d / (2\delta\omega'_r - i\kappa'), \quad (10)$$

where  $\delta\omega'_r = \delta\omega_r + 2\bar{\chi} \langle\sigma_z\rangle$  is the DQD-renormalised detuning. With this choice, Eq. 7 describes an effective undriven resonator, which will relax to a low energy state with  $\langle\tilde{a}^\dagger\rangle = \langle\tilde{a}\rangle = 0$  and  $\langle\tilde{a}^\dagger \tilde{a}\rangle \ll |\alpha|^2$ , as long as  $\kappa' > 0$ .

To find  $P_{e,g}$ , we trace Eq. 2 over resonator degrees of freedom, so that it reduces to the DQD master equation

$$\begin{aligned} \dot{\rho}_q &= -i[\tilde{H}_q, \rho_q] + \gamma_{\downarrow} \mathcal{D}[\sigma_-] \rho_q + \gamma_{\uparrow} \mathcal{D}[\sigma_+] \rho_q \\ &+ \gamma_{\varphi} \mathcal{D}[\sigma_z] \rho_q + \mathcal{L}_{\text{leads}} \rho_q \end{aligned} \quad (11)$$

where

$$\begin{aligned} \tilde{H}_q &= -(\omega_q - 2\bar{\chi}(1 + 2|\alpha|^2)) \sigma_z / 2, \\ \gamma_{\downarrow} &= \gamma_{\downarrow,2} + |\alpha|^2 \gamma_{\downarrow-}^{(\omega_q + \omega_r)} + (|\alpha|^2 + 1) \gamma_{\downarrow+}^{(\omega_q - \omega_r)}, \\ \gamma_{\uparrow} &= \gamma_{\uparrow,2} + |\alpha|^2 \gamma_{\uparrow-}^{(-\omega_q + \omega_r)} + (|\alpha|^2 + 1) \gamma_{\uparrow+}^{(-\omega_q - \omega_r)}, \\ \gamma_{\varphi} &= \gamma_{\varphi,2} + |\alpha|^2 (\gamma_{\varphi-}^{(\omega_r)} + \gamma_{\varphi+}^{(-\omega_r)}). \end{aligned} \quad (12)$$

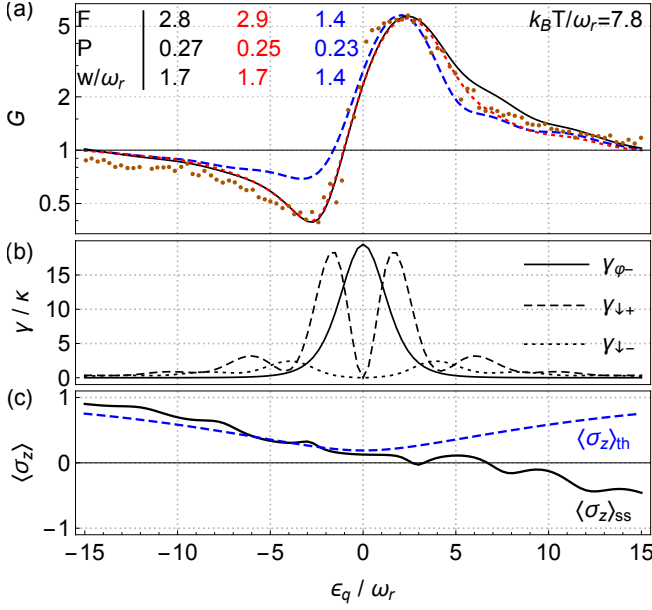


Figure 3. (Color online) **(a)** Logarithmic plot of the microwave power gain,  $G$ , versus DQD bias,  $\epsilon_q$ , for  $k_B T / \omega_r = 7.8$  (corresponding to  $T = 3$  K). Points are experimental data extracted from Ref. 7. The blue-dashed theory curve is generated using terms in the first two lines of Eq. 4, corresponding to the polaron transformation used in Ref. 16. The solid-black theory curve is generated using the six terms in Eq. 4. The dotted red curve includes additional terms discussed in [17]. **(b)** Correlated rates,  $\gamma_{\downarrow+}$  (dashed),  $\gamma_{\downarrow-}$  (dotted), and  $\gamma_{\varphi-}$  (solid) from Eq. 5 corresponding to the black curve in panel (a). **(c)** Qubit steady state population  $\langle \sigma_z \rangle_{ss}$  (solid, black), compared to thermal population of the DQD,  $\langle \sigma_z \rangle_{th}$  (dashed, blue). Common parameters for all panels:  $\omega_d / \omega_r = 1$ ,  $g / \omega_r = 0.0125$ ,  $\Delta_q / \omega_r = 3$ ,  $\kappa / \omega_r = 52 \times 10^{-6}$ ,  $\Gamma / \omega_r = 0.34$ , as in Ref. 16.

The steady-state resonator amplitude,  $\alpha$ , in Eq. 10 is found by solving Eq. 11 for  $P_{e,g}$ , subject to  $\dot{\rho}_q = 0$ .

The power gain due to the DQD coupling is given by

$$G = |\alpha / \alpha_0|^2 = |2\delta\omega_r - i\kappa|^2 / |2\delta\omega'_r - i\kappa'|^2$$

where  $\alpha_0 = -\epsilon_d / (2\delta\omega_r - i\kappa)$  is the steady-state resonator field that would be produced in the absence of the DQD coupling, (i.e. setting  $g = 0$ ). Below, we set  $\delta\omega_r = 0$ , corresponding to resonant cavity driving.

For comparison with experimental gain data extracted from [7], shown as points in Fig. 3a, we assume the bath spectral function is  $C(\omega) = J(\omega)(n_{th} + \theta(\omega))$  with  $J(\omega) = J_{1D}(\omega) + J_{3D}(\omega)$ , where the spectral densities for the first phonon mode in the quantum wire and the piezoelectric substrate phonons are given by [2, 16]

$$\begin{aligned} \frac{J_{1D}(\omega)}{\omega_r} &= F \frac{c_n}{\omega d} (1 - \cos(\omega d / c_n)) e^{-\omega^2 a^2 / 2c_n^2}, \\ \frac{J_{3D}(\omega)}{\omega_r} &= P \frac{\omega}{\omega_r} (1 - \text{sinc}(\omega d / c_s)) e^{-\omega^2 a^2 / 2c_s^2}, \end{aligned} \quad (13)$$

with the speed of sound in the quantum wire  $c_n = 4000$  m/s and in the substrate  $c_s = 11000$  m/s, an inter-dot spacing  $d = 120$  nm and nanowire width  $a = 25$  nm. We treat the dimensionless spectral strengths  $F$  and  $P$  as free parameters, and we tune them so that all theory curves satisfactorily replicate the strong gain peak evident for  $\epsilon_q > 0$ . The specific values are shown in Fig. 3a. As in Ref. 16, we convolve the bare theory gain curves with a normalised gaussian smoothing kernel  $\propto e^{-\epsilon_q^2 / 2w^2}$  to account for low-frequency noise in the gate voltages defining the inter-dot bias [25].

In addition to experimental data, Fig. 3a shows three different theoretical curves. The dashed blue curve includes terms in Eq. 4a,b but not Eq. 4c (i.e. the fourth-order theory restricted to  $\gamma_{\varphi\pm}^{(\mp\omega_r)} = 0$ ), which is equivalent to the polaronic theory in [16]. The solid black curve further includes terms Eq. 4c, corresponding to the DQD-mediated photon to phonon interconversion. The dotted red curve includes all 21 fourth-order rates that appear in the derivation of the full master equation, described in our companion paper Ref. 17.

In Fig. 3a, there is a clear discrepancy between the polaronic theory (blue, dashed) and the experimental data in the regime  $\epsilon_q / \omega_r \lesssim 0$ : the theory does not explain the depth of loss (sub-unity gain). In contrast, the additional dephasing-mediated processes in Eq. 4c (black) give rise to enhanced losses beyond the polaronic terms, and are sufficient to quantitatively account for the entire range of gain and loss observed in the experimental data. We have also shown the results of the full fourth-order theory from Ref. 17 (red dotted). In the parameter regime described here, the difference between the latter two theories is negligible, apart from a rescaling of  $F$  and  $P$ .

Fig. 3b plots the rates in Eq. 5, and shows clearly that the dephasing-assisted loss rate (black),  $\gamma_{\varphi-}^{(\omega_r)}$ , is significant compared to the other correlated decay processes,  $\gamma_{\downarrow\pm}^{(\omega_q \mp \omega_r)}$  (red and blue). This is the main reason for the difference between the theory curves in Fig. 3a. Since the full fourth-order theory accounts for the experimental data, we conclude that dephasing-assisted loss is a substantial contribution to the dynamics of the system.

Fig. 3c shows the steady-state DQD population imbalance,  $\langle \sigma_z \rangle$  (black), compared to the thermal equilibrium value,  $\langle \sigma_z \rangle_{th} = \text{Tr}\{\sigma_z e^{-\beta H_S}\} / \mathcal{Z}$  (blue). In conventional gain/loss models, positive values of the difference  $\langle \sigma_z \rangle_{th} - \langle \sigma_z \rangle$  (i.e. population inversion) drive gain, while negative differences drive loss. This is manifest in  $\kappa'_{\pm}$ , where enhancement of  $P_e$  leads to an increase of  $\kappa'_{+}$ , a corresponding decrease in  $\kappa'$ , and thus an overall increase of  $\alpha$ . In contrast, the dephasing-assisted loss contribution to Eq. 9 is independent of the state of the DQD in the limit that  $P_0 \ll 1$ , which is the case here.

We conclude that the new dephasing-mediated gain and loss Lindblad superoperators in Eq. 4c account for substantial additional loss observed in recent experi-

ments. These terms were derived in our companion paper using Keldysh diagrammatic techniques [17], and arise at the same order of perturbation theory as other terms previously derived using a polaron transformation. Synthesising Lindblad and Keldysh techniques to derive higher order dissipative terms is thus a powerful approach to a consistent, quantitative understanding of quantum phenomena in mesoscopic systems. Lifting the simplifying mean-field approximation to study the effects of correlations between the DQD and resonator will be the subject of future work.

We thank J. H. Cole, A. Doherty, M. Marthaler, J. Petta, A. Shnirman, and J. Taylor for discussions.

- 
- [1] J. R. Petta, A. C. Johnson, C. M. Marcus, M. P. Hanson, and A. C. Gossard, “Manipulation of a single charge in a double quantum dot,” *Phys. Rev. Lett.* **93**, 186802 (2004).
  - [2] T. M. Stace, A. C. Doherty, and S. D. Barrett, “Population Inversion of a Driven Two-Level System in a Structureless Bath,” *Phys. Rev. Lett.* **95**, 106801 (2005).
  - [3] J R Petta, A C Johnson, Jacob M Taylor, EA Laird, Amir Yacoby, Mikhail D Lukin, C M Marcus, M P Hanson, and A C Gossard, “Coherent manipulation of coupled electron spins in semiconductor quantum dots,” *Science* **309**, 2180–2184 (2005).
  - [4] Thomas M Stace, Andrew C Doherty, and David J Reilly, “Dynamical Steady States in Driven Quantum Systems,” *Physical Review Letters* **111**, 180602 (2013).
  - [5] J I Colless, X G Croot, Thomas M Stace, Andrew C Doherty, Sean D Barrett, H Lu, A C Gossard, and David J Reilly, “Raman phonon emission in a driven double quantum dot,” *Nature Communications* **5**, 3716 (2014).
  - [6] Anna Stockklauser, Ville F Maisi, Julien Basset, K Cujia, Christian Reichl, Werner Wegscheider, Thomas Markus Ihn, Andreas Wallraff, and Klaus Ensslin, “Microwave Emission from Hybridized States in a Semiconductor Charge Qubit,” *Physical Review Letters* **115**, 046802 (2015).
  - [7] Y Y Liu, K Petersson, J Stehlik, Jacob M Taylor, and J R Petta, “Photon Emission from a Cavity-Coupled Double Quantum Dot,” *Phys. Rev. Lett.* **113**, 036801 (2014).
  - [8] Manas Kulkarni, Ovidiu Cotlet, and Hakan E Türeci, “Cavity-coupled double-quantum dot at finite bias: analogy with lasers and beyond,” *Phys. Rev. B* **90**, 125402 (2014).
  - [9] Michael Marthaler, Y Utsumi, Dmitri S Golubev, Alexander Shnirman, and Gerd Schön, “Lasing without Inversion in Circuit Quantum Electrodynamics,” *Phys. Rev. Lett.* **107**, 093901 (2011).
  - [10] Pei-Qing Jin, Michael Marthaler, Jared H Cole, Alexander Shnirman, and Gerd Schön, “Lasing and transport in a coupled quantum dot–resonator system,” *Physica Scripta* **2012**, 014032 (2012).
  - [11] Y Y Liu, J Stehlik, Christopher Eichler, M J Gullans, Jacob M Taylor, and J R Petta, “Semiconductor double quantum dot micromaser,” *Science* **347**, 285–287 (2015).
  - [12] Y Y Liu, J Stehlik, M J Gullans, Jacob M Taylor, and J R Petta, “Injection locking of a semiconductor double-quantum-dot micromaser,” *Phys. Rev. A* **92**, 053802 (2015).
  - [13] Michael Marthaler, Y Utsumi, and Dmitri S Golubev, “Lasing in circuit quantum electrodynamics with strong noise,” *Phys. Rev. B* **91**, 184515 (2015).
  - [14] Christian Karlewski, Andreas Heimes, and Gerd Schön, “Lasing and transport in a multilevel double quantum dot system coupled to a microwave oscillator,” *Phys. Rev. B* **93**, 045314 (2016).
  - [15] M J Gullans, J Stehlik, Y Y Liu, Christopher Eichler, J R Petta, and Jacob M Taylor, “Sisyphus Thermalization of Photons in a Cavity-Coupled Double Quantum Dot,” *Physical Review Letters* **117**, 056801 (2016).
  - [16] M J Gullans, Y Y Liu, J Stehlik, J R Petta, and Jacob M Taylor, “Phonon-Assisted Gain in a Semiconductor Double Quantum Dot Maser,” *Phys. Rev. Lett.* **114**, 196802 (2015).
  - [17] Clemens Müller and Thomas M Stace, “Deriving Lindblad master equations with Keldysh diagrams: Correlated gain and loss in higher order perturbation theory,” *Physical Review A* **95**, 013847 (2017).
  - [18] C W Gardiner and P Zoller, *Quantum Noise* (Springer, New York, 2000).
  - [19] Y Yamamoto and A Imamoglu, *Mesoscopic Quantum Optics* (John Wiley & Sons, 1999).
  - [20] D F Walls and Gerard J Milburn, *Quantum Optics* (Springer, Berlin, 2008).
  - [21] “A. Shnirman, private communication,” (2016).
  - [22] G. Lindblad, “On the generators of quantum dynamical semigroups,” *Communications in Mathematical Physics* **48**, 119–130 (1976).
  - [23] Jay M Gambetta, Alexandre Blais, Maxime Boissonneault, Andrew A Houck, D I Schuster, and Steven M Girvin, “Quantum trajectory approach to circuit QED: Quantum jumps and the Zeno effect,” *Phys. Rev. A* **77**, 012112 (2008).
  - [24] D H Slichter, Clemens Müller, R Vijay, S. J. Weber, Alexandre Blais, and Irfan Siddiqi, “Quantum Zeno effect in the strong measurement regime of circuit quantum electrodynamics,” *New Journal of Physics* **18**, 053031 (2016).
  - [25] K D Petersson, L. W. McFaul, M. D. Schroer, M. Jung, Jacob M Taylor, Andrew A Houck, and J R Petta, “Circuit quantum electrodynamics with a spin qubit,” *Nature* **490**, 380–383 (2012).